Carbon 135 (2018) 215–223

Contents lists available at ScienceDirect

Carbon

journal homepage: www.elsevier.com/locate/carbon

High efficiency dispersal and strengthening of graphene reinforced aluminum alloy composites fabricated by powder metallurgy combined with friction stir processing

Z.W. Zhang [1], Z.Y. Liu [1], B.L. Xiao, D.R. Ni, Z.Y. Ma*

Shenyang National Laboratory for Materials Science, Institute of Metal Research, Chinese Academy of Sciences, 72 Wenhua Road, Shenyang, 110016, China

ARTICLE INFO

Article history:
Available online 18 April 2018

ABSTRACT

1 wt.% graphene nanoplatelets reinforced 2009Al (GNP/2009Al) composites were fabricated by a combination of powder metallurgy and subsequent multi-pass friction stir processing (FSP). Microstructural examinations showed that the GNP distribution was significantly improved as the number of FSP passes increased, with a uniform dispersion of GNPs achieved after 2 FSP passes. The layered structures of GNPs were well retained and most of the GNP-Al interfaces were clean and well bonded in FSP composites. Tensile tests showed that the strengths and the elongation of the composites increased initially and then decreased, as the number of FSP passes increased from 1 to 4 passes. In particular, the 2-pass FSP composite exhibited a maximum ultimate tensile strength and yield strength of 514 MPa and 398 MPa, an increase of 23.3% and 30.5%, respectively, compared with 2009Al alloy. Moreover, a sound elongation of 10% was obtained for the 2-pass FSP composite. A strength calculation based on load transfer indicated that the high efficiency strengthening of the composite could be attributed to the large specific surface area of uniformly dispersed GNPs.

1. Introduction

Graphene, a new member of the carbon material family, has gained extensive attention due to its excellent mechanical and physical properties [1–4]. With extremely high strength and modulus as well as low density, graphene has been considered as an ideal reinforcement for high-performance composites. Furthermore, the two-dimensional morphology of graphene is more favorable for load transferring compared to fullerene and carbon nanotubes (CNTs). Graphene nanoplatelets (GNPs) with a few layers exhibit similar properties as single layer graphene, but are less expensive and easier to mass produce [5–7]. Therefore, GNPs have been widely used to reinforce various matrices in place of single layer graphene.

In the past few years, numerous GNP reinforced polymer and ceramic matrix composites with enhanced properties have been reported [8–10]. Incorporating GNPs into metal matrices could also lead to high-performance metal matrix composites. However, it is extremely difficult to uniformly disperse GNPs into metal matrices because GNP agglomerations form more easily due to their larger specific surface area compared to that of CNTs.

Recently, several routes have been tested for dispersing GNPs into metal matrices, such as high-energy ball milling (HEBM), molecular-level mixing (MLM), and flake powder metallurgy (Flake PM). By using HEBM, GNPs could be uniformly distributed into metal matrices due to repeated deformation, cold welding, and fracturing of the metal powders [11–17]. However, GNPs were severely damaged and contaminated during milling, which resulted in limited strengthening efficiency and poor ductility [11,12].

By reaction of graphene oxide (GO) nanosheets with metal (Cu, Co, Ni) ions based on MLM, composites with uniformly dispersed reduced GO (rGO) were prepared after hydrogen reduction [18,19]. However, it is difficult to fabricate GNPs reinforced Al matrix (GNP/Al) composites by this method. Using Flake PM, GO nanosheets were firstly absorbed onto metal flakes and then reduced to rGO by heating to a high temperature. Wang et al. [20] fabricated a 0.3 wt.% rGO/Al composite using Flake PM combined with hot extrusion. They found that the tensile strength of the composite was much higher than that of the unreinforced Al matrix. However, many structural defects remained on the surface of rGO.

* Corresponding author.
E-mail address: zyma@imr.ac.cn (Z.Y. Ma).
[1] These two authors contributed equally to this work.

https://doi.org/10.1016/j.carbon.2018.04.029
0008-6223/

Friction stir processing (FSP), is an emerging solid-state metal-working technique based on friction stir welding [21,22]. The material in the processed zone is severely deformed and thoroughly mixed in the solid state. FSP has proven to be an effective method of dispersing reinforcements into metal matrices and homogenizing the microstructure of heterogeneous materials such as cast alloys and composites [23–27]. Liu et al. [25] fabricated CNT/aluminum composites by combining powder metallurgy (PM) and FSP. The CNTs in the 3-pass FSP composites were uniformly dispersed in the Al matrix with well-bonded interfaces. As a result, the mechanical strengths of the composites were significantly improved.

FSP is also expected to be an effective method for fabricating GNP/Al composites. However, GNPs and CNTs have quite different morphologies. The strong van der Waals forces between GNP flakes make GNPs more difficult to disperse than CNTs. Furthermore, the larger aspect ratio of GNPs means greater fracture tendency of GNPs during dispersion. Thus, the feasibility of effectively dispersing GNPs through FSP and achieving GNP/Al composites with well structure integrity and higher tensile properties is worthy of deep investigation.

So far, very limited work has been performed on GNP/Metal composite fabrication by FSP. Khodabakhshi et al. [28] fabricated GNP/Al surface composites by pre-placing GNP powders on Al-Mg plates and conducting 5-pass FSP. The tensile properties were reported to increase after incorporating GNPs by FSP. However, the relationships among number of FSP pass and GNP distribution, structure integrity and tensile properties of composites have not been investigated.

It is important to note that the reported studies on the GNP/Al composites were mostly limited to a pure Al matrix [11,12,16,17,20]. Composites based on a pure Al matrix usually exhibit relatively low mechanical strength (e.g. lower than 400 MPa) [11,12,20,29], limiting their engineering applications.

In this work, a new process combining PM and FSP was developed to prepare GNP/2009Al composites. The influence of FSP passes on GNP distribution, damage, and strengthening of GNP/2009Al composites was investigated. The aim of this work is to establish an effective method for dispersing GNPs into an aluminum alloy matrix yielding composites with excellent strength and good ductility.

2. Experimental

2.1. Raw materials and composite billet fabrication

The GNPs used in this study were produced by the Institute of Metal Research, Chinese Academy of Sciences in the form of graphene paste. Morphologies are shown in Fig. 1(a). After sonicating in ethanol for 1 h, few-layer graphenes were obtained, as shown in Fig. 1(b). The few-layer graphenes were about 2–3 nm in thickness and 5–10 μm in lateral size. As-received 2009Al powders, with nominal composition of Al-4.5 wt.% Cu-1.2 wt.% Mg, shown in Fig. 1(c), had an average diameter of about 8 μm.

Solution-assisted wet mixing was used to distribute GNPs in 2009Al alloy powders. First, the as-received GNPs paste was added to ethanol and sonicated for 1 h to obtain a dispersed GNP suspension. Then, 2009Al powder was gradually added to the GNP suspension with continuously stirring using a mechanical stirrer at a speed of 200 rpm for 2 h. The stirred GNP/2009Al mixture was filtered and dried at 40 °C for 20 h to obtain 1 wt.% GNP/2009Al powders.

The as-mixed 1 wt.% GNP/2009Al powders were cold-compacted in a cylinder die under a pressure of about 10 MPa, degassed under a vacuum of about 5×10^{-3} Pa, and then hot-pressed under a pressure of about 50 MPa at 833 K for 1 h into cylindrical billets with a diameter of 60 mm and a height of 50 mm.

2.2. GNP dispersion by FSP

The as-pressed billets were hot forged at 753 K into disc plates with a thickness of about 10 mm. Then the plates were subjected to 1 to 4-pass in situ FSP at a tool rotation rate of 2000 rpm and a travel speed of 100 mm/min, using a tool with a concave shoulder 20 mm in diameter, a threaded cylindrical pin 6 mm in diameter, and 4.7 mm in length. The as-FSP composites were subjected to a T4-treatment (solutionized at 768 K for 2 h, water quenched, and then naturally aged for 4 days).

2.3. Characterization

GNP distributions in composites under various fabrication conditions were examined using optical microscopy (OM, Zeiss Axiovert 200 MAT), field emission scanning electron microscopy (FESEM, Leo Supra 55), and transmission electron microscopy (Tecnai G2 20). GNP-Al interfaces and GNP structures were observed by high resolution TEM (HRTEM, Tecnai G2 20). Raman spectroscopic measurements were conducted using a JY Labram HR800 (excitation of about 1 μm). The peak intensity ratio of D-line (defect) and G-line (graphite), I_D/I_G, was calculated to quantify the disordering and defect density in graphitic structures. An X-ray diffraction (XRD) analyzer (D/max 2400) was used to identify the phases of the composites. Composite densities were measured at room temperature by the Archimedean principle. Distilled water was used as the liquid for the measurement and at least three specimens were tested to obtain an accurate average value.

The Vickers microhardness (HV) of composites was measured using a Leco-LM-247 AT indenter under a load of 1000 g with a dwell time of 30 s. Dog-bone tensile specimens with a gauge length of 5.0 mm, a width of 1.5 mm, and a thickness of 1.0 mm were machined from FSP composites parallel to the FSP direction and from the forged composite parallel to the radial direction. Tensile tests were conducted at a strain rate of 1×10^{-3} s^{-1} at room temperature using an Instron 5848 microtester. At least four specimens were tested for each composite. The fracture surfaces of the composites were observed using FESEM (Leo Supra 55).

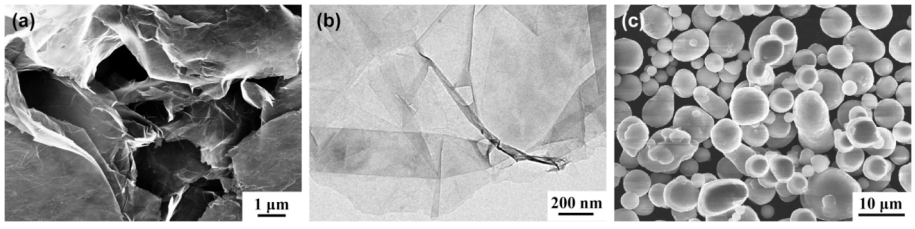

Fig. 1. Morphologies of (a) as-received GNPs, (b) few-layer graphenes, and (c) as-received 2009Al powders. (A colour version of this figure can be viewed online.)

3. Results and discussion

3.1. GNP distributions

Fig. 2 shows the cross-sectional macrographs of the FSP composites and the hardness profiles along the mid-depth of the processed zones (PZs). The hardness of the PZ after 1-pass FSP was significantly increased compared with that of the forged composite (Fig. 2(d)). After two or more FSP passes, hardness values were relatively uniform throughout the PZ (Fig. 2(e) and (f)). However, after 4 passes HV hardness values were slightly lower than those after 2 passes.

Fig. 3 shows SEM images of GNP distributions in T4-treated 1 wt.% GNP/2009Al composites under different processing conditions. For the forged composite, GNP clusters were aligned parallel to the radius of the forged disc plates, as shown by arrows in Fig. 3(a). This is because the aluminum matrix underwent large plastic deformation in the radial direction during hot forging, resulting in GNP clusters moving along with the matrix, forming a straight and parallel radial distribution of GNP clusters.

Under larger magnification, GNP clusters with many flakes stacked together were clearly observed (Fig. 3(b)). This indicates that the mixing and forging processes were not effective enough to disperse GNPs into the aluminum matrix due to strong inter-layer Van der Waals interactions. However, after 1-pass FSP, the large GNP clusters were significantly reduced, leaving only much smaller clusters (Fig. 3(c)). After 2 or more FSP passes (Fig. 3(d), (e) and (f)), no GNP clusters were observed by SEM. Some white particles were observed in all of the composites, which are the residual Al_2Cu phase after solid solution treatment, as identified by XRD diffraction pattern in Fig. 6.

Fig. 4 shows GNP distributions of 2- and 4-pass FSP composites under TEM. For the 2-pass FSP composite (Fig. 4(a)), GNPs with a lateral size of about 500 nm were significantly broken up compared to the forged composite (Fig. 3(b)), and were uniformly dispersed in the aluminum matrix. Further increasing the number of FSP passes resulted in even smaller GNP sizes, as shown in Fig. 4(b), with a lateral size of about 100 nm for the 4-pass FSP composite. This indicates that GNPs were uniformly dispersed into the aluminum matrix due to the intense stirring of FSP.

3.2. GNP structure

Fig. 5 shows Raman spectra of the 1 wt.% GNP/2009Al powders and GNP/2009Al composites under different conditions. The relative peak intensity ratios of D-band to G-band (I_D/I_G) are summarized in Table 1. The Raman spectra of GNP/2009Al powders show a D-band at 1336 cm^{-1}, a G-band at 1580 cm^{-1}, and a 2D-band at 2660 cm^{-1}, with an I_D/I_G ratio of 0.16, indicating the typical graphene structure with low defect density [30]. After sonication pretreatment, hot pressing, and forging, the I_D/I_G ratio increased to 0.82, indicating the introduction of a number of defects or disorders to the graphene structure.

The I_D/I_G ratio increased from 0.82 to 1.16 after one pass of FSP. As the number of FSP passes increased from one to four, the I_D/I_G ratio increased from 1.16 to 1.41, indicating that FSP caused some damage to GNPs. This is in accordance with observation of the GNP structure. As the number of FSP passes increased, the GNP size was reduced, resulting in more edges and defects in GNPs. However, due to a short application duration and relatively low energy input, GNP damage during FSP was mild compared to high-energy ball milling [11,12,14].

The peak position of the G-band (w_G) implies the stress states in graphene [31]. When graphene was strained, the interatomic distance of graphene changed. Hence, the vibrational frequency of the G-band changed, leading to a wavenumber shift. In this study, the wavenumbers of GNPs in GNP/2009Al powders and the as-forged composite were almost the same (1580 cm^{-1} versus 1578 cm^{-1}). This indicates that GNPs did not experience significant stress during hot pressing and hot forging. After 1-pass FSP, however, the wavenumber increased from 1578 cm^{-1} to 1602 cm^{-1}, indicating reduced interatomic distances in GNPs. This means that residual compressive stresses increased in FSP composites. The wavenumber did not change with more FSP passes, indicating that increased numbers of FSP passes did not introduce severer stress to GNPs.

Fig. 6 shows the XRD pattern of the T4 treated 1 wt.% GNP/2009Al composites. In addition to peaks of Al and Al_2Cu that is the strengthening phase in Al-Cu alloys, a weak peak corresponding to (009) diffraction of Al_4C_3 was detected in the forged composite. This indicates that slight reaction between GNPs and Al occurred during fabrication and heat treatment. After 2-pass FSP, the peak corresponding to (009) diffraction of Al_4C_3 did not intensify and no other peaks of Al_4C_3 appeared. This indicates that FSP did not aggravate the interface reaction between GNPs and Al significantly. It is thought that carbon atoms at the defect sites of GNPs would react with Al at high temperature, forming Al_4C_3 during composite fabrication and forging. Although FSP further increased the number

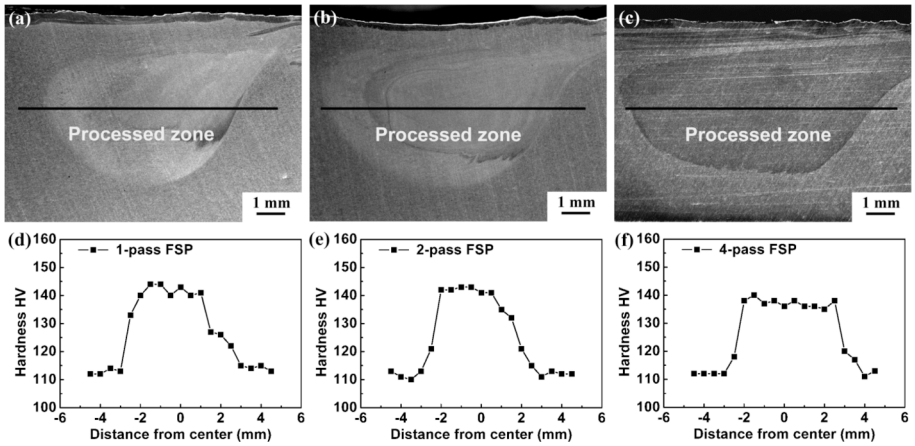

Fig. 2. OM images and hardness profiles of FSP 1 wt.% GNP/2009Al composites: (a) (d) 1-pass FSP, (b) (e) 2-pass FSP, (c) (f) 4-pass FSP. (A colour version of this figure can be viewed online.)

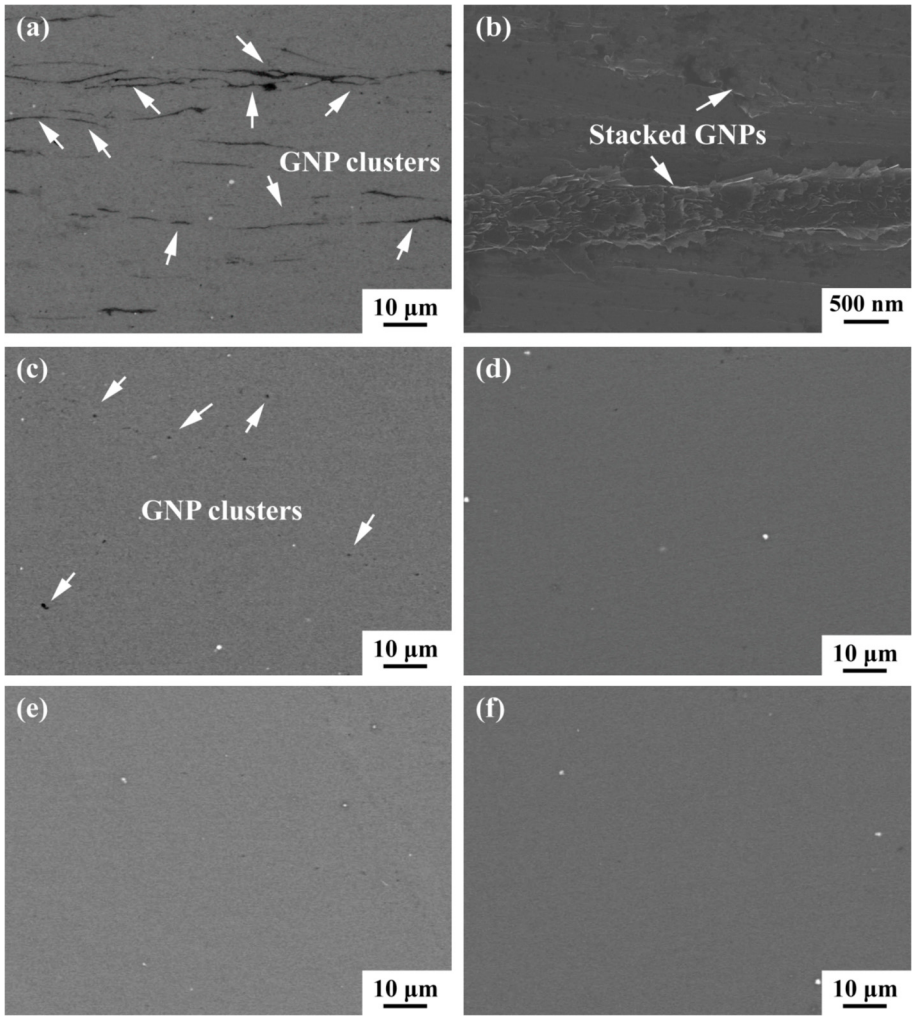

Fig. 3. SEM images showing GNP distributions in T4-treated 1 wt.% GNP/2009Al composites: (a)(b) forged, (c) 1-pass FSP, (d) 2-pass FSP, (e) 3-pass FSP, and (f) 4-pass FSP. (A colour version of this figure can be viewed online.)

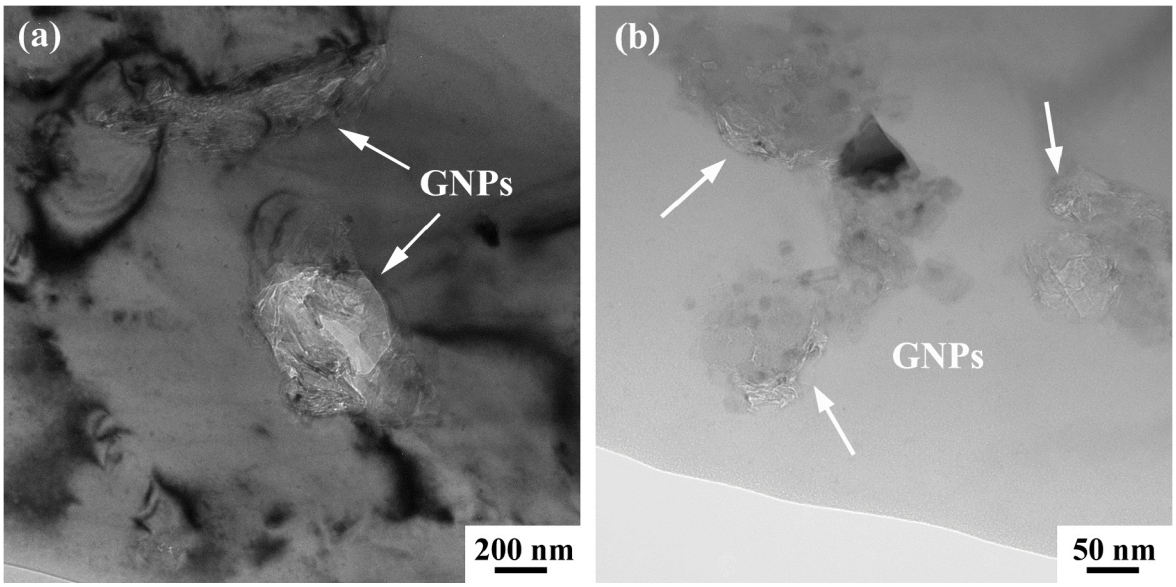

Fig. 4. TEM images showing GNP distributions in 1 wt.% GNP/2009Al composites: (a) 2-pass FSP and (b) 4-pass FSP. (A colour version of this figure can be viewed online.)

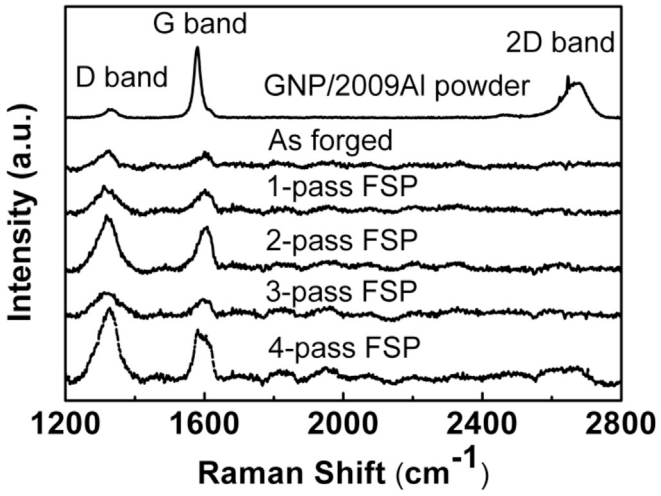

Fig. 5. Raman spectra of 1 wt.% GNP/2009Al powders and composites under different conditions. (A colour version of this figure can be viewed online.)

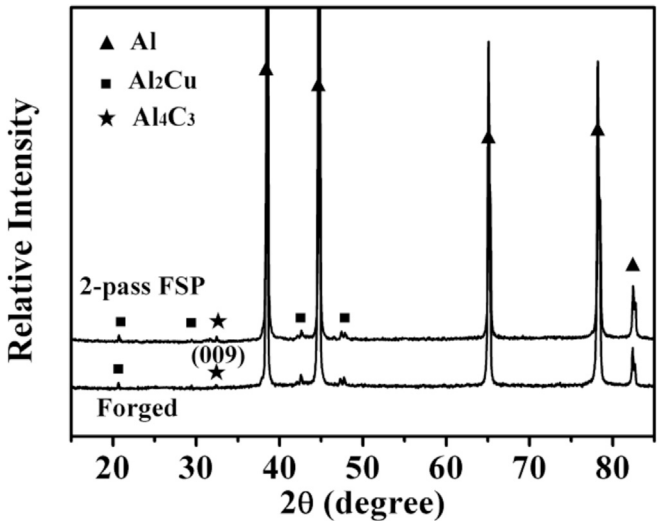

Fig. 6. XRD patterns of T4 treated 1 wt.% GNP/2009Al composites. (A colour version of this figure can be viewed online.)

of defect sites as GNPs were broken into small pieces, the interfacial reaction between GPNs and Al was not significantly enhanced because of low process temperature and short duration of FSP.

HRTEM observations indicated that the GNP-Al interfaces in the 2-pass FSP composite were well bonded without micro-void (Fig. 7(a) and (b)). Generally, GNPs were difficult to wet by most of the liquid metals. However, the severe plastic deformation during FSP could induce large pressure between GNP and Al matrix at a high temperature, resulting in the formation of good GNP-Al bonding. This phenomenon has also been reported in other non-wettable systems, e.g., CNT-Al [24], SiC-Al [32] during FSP. The inter-layer distance of few-layer graphene was ~0.324 nm (Fig. 7(b)), similar to that of graphite, indicating the good structure integrity of GNPs. Furthermore, wrinkled GNP (Fig. 7(a)) and curved GNP (Fig. 7(c)) were also observed in the Al matrix. This is attributed to the extremely large ratio of lateral dimension to thickness of GNPs and the complex material flow during FSP. Al_4C_3, with a length of about 200 nm, was occasionally detected near GNPs in composites, as shown in Fig. 7(d), indicating the occurrence of slight interfacial reaction between GNPs and Al, consistent with the XRD results (Fig. 6). It has been reported that a small amount of Al_4C_3 could enhance the CNT-Al bonding [33]. Thus, it is believed that the slight GNP-Al reaction was beneficial to enhancing the interface bonding of GNP-Al, similar with that of CNT-Al [33].

3.3. Mechanical properties of GNP/2009Al

Table 2 shows the densities and tensile properties of T4-treated 2009Al alloy and GNP/2009Al composites under different conditions. The 2009Al alloys were fabricated in our previous study [25] using the same process as the GNP/2009Al composites. The densities and tensile properties of the 2009Al alloys under forged or different FSP conditions were almost the same. This indicates that the forged 2009Al alloy was dense and exhibited sound tensile properties, and therefore subsequent FSP passes would not improve the density and mechanical properties further.

The GNP/2009Al composites exhibited significant difference between forged and FSP conditions. The forged composite had the lowest density and tensile properties. This is attributed to internal voids in the GNP clusters, formed because the aluminum matrix could not enter the clusters easily (Fig. 3(a) and (b)). This not only resulted in a lower density, but also deteriorated the mechanical properties of the composite. Under tension, the stress was concentrated at the GNP clusters and voids, resulting in poor strength and ductility of forged composite, as shown in Fig. 8. The strength of forged composite was even lower than that of the 2009Al alloy.

After 1 pass of FSP, density and tensile properties increased significantly due to reduced number and size of voids and an improved GNP distribution. After 2 passes of FSP, composites reached their maximum strength, with a yield strength (YS) of 398 MPa and an ultimate tensile strength (UTS) of 514 MPa. Moreover, elongation of FSP composites was much higher than that of forged composite (Table 2 and Fig. 8), and a 10% elongation was achieved with the 2-pass FSP composite. This can be attributed to three causes. First, GNPs were uniformly dispersed in the aluminum matrix. This eliminated GNP clusters and reduced voids in the matrix. Second, GNP-Al interfaces were clean and well-bonded, despite Al_4C_3 being occasionally detected near GNPs. Third, no contamination, such as Al_2O_3 or Fe, was introduced during fabrication, which is known to be a significant problem in HEBM [11,12].

Compared with the FSP 2009Al alloy, the 2-pass FSP composite showed an obvious increase in strength. The YS and UTS of the 2-pass FSP composite increased by 30.5% and 23.3%, respectively. This indicates that uniformly dispersed 1 wt.% GNPs with good interfacial bonding with the Al matrix significantly strengthened

Table 1
I_D/I_G and Raman G-band peak positions of GNPs in 1 wt.% GNP/2009Al powders and composites under different conditions.

State	Composite powder	Forged composite	FSP composite			
			1-pass	2-pass	3-pass	4-pass
I_D/I_G	0.16	0.82	1.16	1.22	1.39	1.41
w_G (cm^{-1})	1580	1578	1602	1608	1601	1600

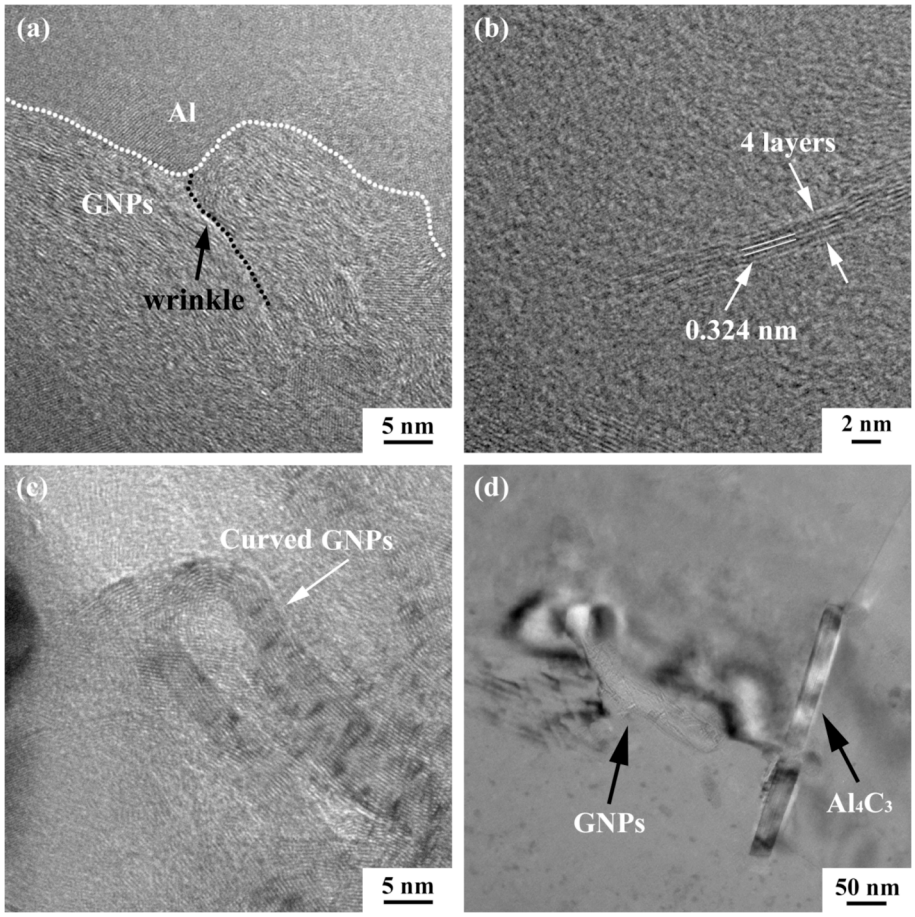

Fig. 7. HRTEM images of 2-pass FSP composite showing (a) GNP-Al interface and wrinkled GNP, (b) few-layer graphene, (c) curved GNPs, and (d) TEM image of Al_4C_3 in Al matrix near GNPs. (A colour version of this figure can be viewed online.)

Table 2
Densities and tensile properties of T4-treated 2009Al and GNP/2009Al composites.

Specimen	Condition	Density (g/cm^3)	YS (MPa)	UTS (MPa)	El. (%)
2009Al alloy [26]	Forged	2.757	299	411	12
	1-pass FSP	2.755	297	421	13
	4-pass FSP	2.760	305	417	15
1 wt.% GNP/2009Al	Forged	2.661	251	272	1
	1-pass FSP	2.717	314	398	4
	2-pass FSP	2.746	398	514	10
	3-pass FSP	2.745	378	468	7
	4-pass FSP	2.746	363	462	8

[a]Theoretical density of 2009Al is ~2.750 g/cm^3 and that of GNP is ~2.250 g/cm^3 [34].
[b]Theoretical density of 1.0 wt.% GNP/2009Al is ~2.744 g/cm^3.

the Al alloy.

Further increasing the number of FSP passes from 2 to 3 or 4 resulted in declined strength and elongation. This is attributed to the reduced GNP size (about 100 nm for the 4-pass FSP composite, Fig. 4(b)) after too many FSP passes. This will be discussed later in detail.

Fig. 9 shows typical fractographs of GNP/2009Al composites under different conditions. For the forged composite, the aluminum matrix with a layered morphology was observed (Fig. 9(a)). GNP clusters with a lateral size of about 10 μm were distributed between the layer matrices. The aluminum matrix was interrupted by large aligned GNP clusters, which resulted in a brittle fracture without apparent dimples. Fig. 9(b) and (c) confirmed that GNPs were dispersed homogeneously in the aluminum matrix after FSP. Uniform and fine dimples were observed, in accordance with the relatively high elongations of 10% and 8% for the 2-pass and 4-pass FSP composites, respectively. Moreover, GNPs on the fracture surface of the 2-pass FSP composite (Fig. 9(b)) exhibited a significantly larger lateral size than those of the 4-pass FSP composite, in accordance with TEM observations (Fig. 4).

3.4. Strengthening of composites by GNPs

For composites reinforced with short fibers or whiskers, an applied force is transferred form the matrix to the reinforcement by shear stress developed along the fiber/matrix interface [35]. Considering the high specific surface area of GNPs, a modified shear-lag model developed by Shin et al. [17] was used to evaluate

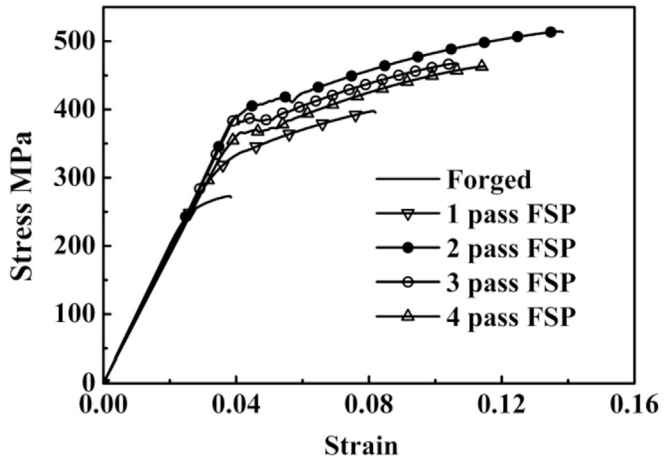

Fig. 8. Stress-strain curves of T4-treatd 1 wt.% GNP/2009Al composites under different conditions. (A colour version of this figure can be viewed online.)

the strengthening effect of the composites.

For GNP reinforced composites, the force balance between the interfacial shear stress and reinforcement tensile stress can be expressed as:

$$(wt)d\sigma_p = \tau_m\{2(w+t)\}dx \tag{1}$$

where w is the width of a GNP, t is the thickness of a GNP, σ_p is the (position specific) tensile stress of a GNP, τ_m is the shear strength of the matrix (about 0.5 σ_m, σ_m is the tensile YS of the matrix), and x is the distance from the end of a GNP. Assuming that the length of a given GNP is l, the cross-section area (A) and the interfacial area (S) of GNP are wt and $2(w+t)l$, respectively. In this case, Eq. (1) can be expressed as:

$$d\sigma_p = \frac{S}{Al}\tau_m dx \tag{2}$$

This formula implies that the tensile stress of a GNP is maximum at its mid-length and zero at its ends. There is a critical length (l_c) for GNPs when the maximum stress reaches the tensile strength of GNPs. If the GNP length is less than the critical length ($l < l_c$), the tensile stress of GNPs is proportionally increased with GNP length. Otherwise, when GNP length exceeds the critical length ($l > l_c$), GNP has a stress equal to its tensile strength over a certain length ($l - l_c$). The critical length of GNP, l_c, can be calculated as:

$$l_c = \sigma_r\frac{Al}{\tau_m S} \tag{3}$$

where σ_r is the YS of the reinforcements, which is 30 GPa for GNPs [36]. The YS of the 2009Al matrix is about 305 MPa, t is the thickness of GNPs, which is about 3 nm. As the thickness of GNPs is far less than their width (about 500 nm and 100 nm in the 2- and 4-pass FSP composites, respectively), Eq. (3) can be simplified as:

$$l_c = \frac{t\sigma_r}{2\tau_m} \tag{4}$$

The calculated l_c value for GNPs in this study is about 300 nm, which is smaller than that for the 2-pass FSP composite and larger than that for the 4-pass FSP composite. In this case, the theoretical strength for the 2- and 4-pass FSP composites can be expressed as Eq. (5) and Eq. (6), respectively.

$$\sigma_c = \sigma_r V_r\left(1 - \frac{l_c}{2l}\right) + \sigma_m V_m \tag{5}$$

$$\sigma_c = \sigma_r V_r\left(\frac{l}{2l_c}\right) + \sigma_m V_m \tag{6}$$

where V_r and V_m are the volume fraction of GNPs (1.2 vol.%, namely 1.0 wt.%) and the matrix, respectively.

According to Eqs. (5) and (6), the calculated YS of the 2- and 4-pass FSP composites are 548 MPa and 356 MPa, respectively. It is noted that the calculated value for the 4-pass FSP composite was in good agreement with the experimental result (363 MPa), demonstrating that the GNP-Al bonding was strong enough (at least larger

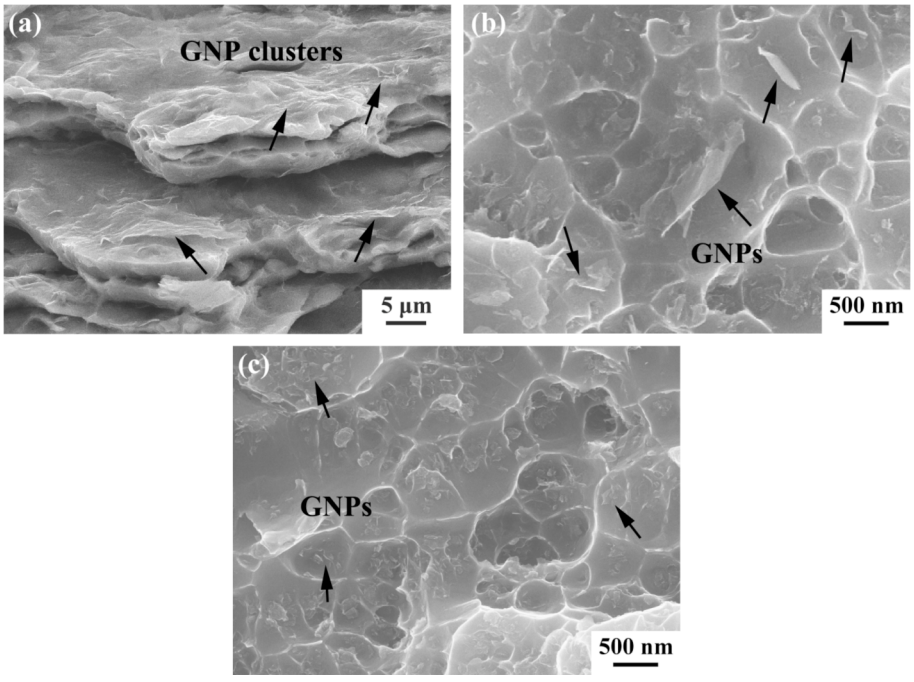

Fig. 9. Fractographs of 1 wt.% GNP/2009Al composites: (a) forged, (b) 2-pass FSP, and (c) 4-pass FSP. (A colour version of this figure can be viewed online.)

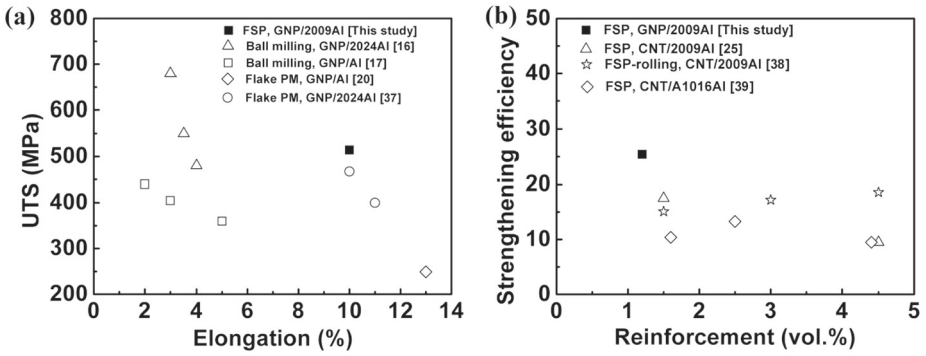

Fig. 10. (a) Strength-ductility comparison of GNP/Al composites fabricated by various processes and (b) strengthening efficiency of GNP/Al and CNT/Al composites fabricated by FSP [37,38,39]. (A colour version of this figure can be viewed online.)

than the strength of Al matrix) and the strength of the 4-pass FSP composite could be well predicted for GNPs of an ideal distribution. However, for the 2-pass FSP composite, the calculated value (~548 MPa) was much higher than the experimental data (~398 MPa), which could be attributed to following causes. First, the calculated model was based on the perfect alignment of reinforcements in the loading direction. However, GNPs in the FSP composites were randomly oriented. Second, as the GNP size increased, curved GNPs, as seen in Fig. 7(c), were induced. The random orientation and curving morphology of GNPs would result in a reduced effective length for load transfer and thus severely reduce load transferring efficiency. In this case, the strengthening effect was reduced, leading to overestimation in the strengthening calculation for the 2-pass FSP composite.

It should be pointed out that the experimental strength of the 2-pass FSP composite was 398 MPa, which was even lower than the calculated strength (~476 MPa) of the composite with a critical length (l_c ~300 nm) of GNPs according to Eq. (5). This means that the effective length of GNPs for load transfer in the 2-pass FSP composite should be smaller than the l_c, though the actual length of GNPs was larger than the l_c. This implies that the maximum tensile stress of a GNP at its mid-length would not reach the fracture strength. So on the whole, most of the GNPs on the fractograph (Fig. 9(b)) were considered as pulled-out GNPs rather than cracked GNPs. It is expected that a much higher strengthening efficiency can be achieved by aligning and flattening GNPs in the matrix.

Furthermore, the calculated YS (~548 MPa) of the 2-pass FSP composite with a large lateral size (~500 nm) was much higher than that of the 4-pass FSP composite (~356 MPa) with a small lateral size (~100 nm). This indicates that the GNP lateral size related with interfacial area had a significant influence on strengthening. The large lateral size of GNPs could effectively transfer load through their interfaces. Reducing damage to GNPs by ensuring a uniform GNP distribution is critically important to increasing composite strengths. Clearly, more in-depth studies are needed to reduce the damage to GNPs during fabrication of GNP/Al composites.

The strength and elongation of GNP reinforced pure Al and aluminum alloy composites fabricated by various dispersing processes are compared in Fig. 10(a). The composite fabricated by FSP exhibited a much better combination of strength and ductility due to the uniform GNP distribution, less contamination, and good bonding of GNP-Al interface.

The YS of the metal matrix composites can be expressed as:

$$\sigma_c = \sigma_m(1 + V_r R) \tag{7}$$

where R is the strengthening efficiency of reinforcement. Large value of the strengthening efficiency means high strengthening ability due to reinforcement incorporation. For GNP/Al and CNT/Al composites, the strengthening efficiency could be expressed as follows according to Eqs. (3) and (6):

$$R = \frac{l}{4}\frac{S}{V} - 1 \tag{8}$$

where V is the volume of GNPs or CNTs. Eq. (8) demonstrates that the strengthening efficiency of GNPs or CNTs was greatly affected by the specific surface area ($\frac{S}{V}$). The strengthening efficiency of GNP/Al and CNT/Al composites fabricated by FSP are compared in Fig. 10(b). It is clear that GNPs exhibited a higher strengthening efficiency than CNTs, which was mainly attributed to the flake GNPs providing a larger specific surface area than CNTs.

4. Conclusions

(1) GNPs were dispersed in an aluminum matrix by a combination of PM and FSP. As the number of FSP passes increased, the number and size of GNP clusters decreased and a homogeneous GNP distribution was achieved by 2-pass FSP.
(2) The lateral size of GNPs decreased with increasing the number of FSP passes. GNPs with average lateral sizes of about 500 nm and 100 nm were observed in the 2- and 4-pass FSP composites, respectively. The layer structures of GNPs were well retained and most of the GNP-Al interfaces were well bonded in FSP composites, though Al_4C_3 was occasionally detected near GNPs.
(3) The FSP 1 wt.% GNP/2009Al composites exhibited excellent tensile properties. In particular, the 2-pass FSP composites exhibited the best strengthening effect, with YS and UTS increased by 30.5% and 23.3%, respectively, compared with the FSP 2009Al alloy. The 2-pass FSP composite also exhibited a relatively high elongation of 10%. Further increasing the number of FSP passes from 2 to 3 or 4 resulted in declined strength and ductility.
(4) Strength calculations based on load transfer indicated that the high efficiency strengthening of composites was mainly attributed to the large specific surface area of uniformly dispersed GNPs.

Acknowledgements

The authors gratefully acknowledge the support of (a) the National Natural Science Foundation of China (grant No. 51501189), (b) Key Research Program of Frontier Sciences, CAS, (c) the Aeronautical Science Foundation of China (grant No. 2016ZF54030), and (d) CAS/SAFEA International Partnership Program for Creative Research Teams.

References

[1] A.K. Geim, K.S. Novoselov, The rise of graphene, Nat. Mater. 6 (3) (2007) 183–191.
[2] C. Lee, X. Wei, J.W. Kysar, J. Hone, Measurement of the elastic properties and intrinsic strength of monolayer graphene, Science 321 (5887) (2008) 385–388.
[3] A.A. Balandin, S. Ghosh, W. Bao, I. Calizo, D. Teweldebrhan, F. Miao, et al., Superior thermal conductivity of single-layer graphene, Nano Lett. 8 (3) (2008) 902–907.
[4] M. Orlita, C. Faugeras, P. Plochocka, P. Neugebauer, G. Martinez, D.K. Maude, et al., Approaching the Dirac point in highmobility multilayer epitaxial graphene, Phys. Rev. Lett. 101 (26) (2008) 973–980.
[5] S. Stankovich, D.A. Dikin, G.H.B. Dommett, K.M. Kohlhaas, E.J. Zimney, et al., Graphene-based composite materials, Nature 442 (2006) 282–286.
[6] N.A. Kotov, Carbon sheet solutions, Nature 442 (2006) 254–255.
[7] R.D. Pinera, S.T. Nguyenb, R.S. Ruoffa, Synthesis and exfoliation of isocyanate-treated graphene oxide nanoplatelets, Carbon 44 (15) (2007) 3342–3347.
[8] X. Zhao, Q. Zhang, D. Chen, Enhanced mechanical properties of graphene-based poly (vinyl alcohol) composites, Macromolecules 43 (5) (2010) 2357–2363.
[9] S. Vadukumpully, J. Paul, N. Mahanta, S. Valiyaveettil, Flexible conductive graphene/poly(vinyl chloride) composite thin films with high mechanical strength and thermal stability, Carbon 49 (1) (2011) 198–205.
[10] H. Porwal, P. Tatarko, S. Grasso, J. Khaliq, I. Dlouhý, M.J. Reece, Ceramic. Graphene reinforced alumina nano-composites, Carbon 64 (2013) 359–369.
[11] S.F. Bartolucci, J. Paras, M.A. Rafiee, J. Rafiee, S. Lee, D. Kapoor, et al., Graphene–aluminum nanocomposites, Mater. Sci. Eng., A 528 (27) (2011) 7933–7937.
[12] R. Pérez-Bustamante, D. Bolaños-Morales, J. Bonilla-Martínez, I. Estrada-Guel, R. Martínez-Sánchez, Microstructural and hardness behavior of graphene nanoplatelets/aluminum composites synthesized by mechanical alloying, J. Alloy. Comp. 615 (2014) S578–S582.
[13] X. Gao, H.Y. Yue, E. Guo, H. Zhang, X.Y. Lin, L.H. Yao, et al., Mechanical properties and thermal conductivity of graphene reinforced copper matrix composites, Powder Technol. 301 (2016) 601–607.
[14] H. Yue, L. Yao, X. Gao, et al., Effect of ball-milling and graphene contents on the mechanical properties and fracture mechanisms of graphene nanosheets reinforced copper matrix composites, J. Alloy. Comp. 691 (2017) 755–762.
[15] W.J. Kim, T.J. Lee, S.H. Han, Multi-layer graphene/copper composites: preparation using high-ratio differential speed rolling, microstructure and mechanical properties, Carbon 69 (2014) 55–65.
[16] S.E. Shin, D.H. Bae, Deformation behavior of aluminum alloy matrix composites reinforced with few-layer graphene, Composites 78 (2015) 42–47.
[17] S.E. Shin, H.J. Choi, J.H. Shin, D.H. Bae, Strengthening behavior of few-layered graphene/aluminum composites, Carbon 82 (2015) 143–151.
[18] J. Hwang, T. Yoon, S.H. Jin, J. Lee, T.S. Kim, S.H. Hong, et al., Enhanced mechanical properties of graphene/copper nanocomposites using a molecular-level mixing process, Adv. Mater. 25 (46) (2013) 6724–6729.
[19] F.Y. Chen, J.M. Ying, Y.F. Wang, S.Y. Du, Z.P. Liu, Q. Huang, Effects of graphene content on the microstructure and properties of copper matrix composites, Carbon 96 (2016) 836–842.
[20] J. Wang, Z. Li, G. Fan, H. Pan, Z. Chen, D. Zhang, Reinforcement with graphene nanosheets in aluminum matrix composites, Scripta Mater. 66 (8) (2012) 594–597.
[21] R.S. Mishra, Z.Y. Ma, Friction stir welding and processing, Mater. Sci. Eng. R 50 (2005) 1–78.
[22] K. Zhao, Z.Y. Liu, B.L. Xiao, Z.Y. Ma, Friction stir welding of carbon nanotubes reinforced Al-Cu-Mg alloy composite plates, J. Mater. Sci. Technol. 33 (9) (2017) 1004–1008.
[23] Z.Y. Ma, A.L. Pilchak, M.C. Juhas, J.C. Williams, Microstructural refinement and property enhancement of cast light alloys via friction stir processing, Scripta Mater. 58 (5) (2008) 361–366.
[24] H. Izadi, A.P. Gerlich, Distribution and stability of carbon nanotubes during multi-pass friction stir processing of carbon nanotube/aluminum composites, Carbon 50 (12) (2012) 4744–4749.
[25] Z.Y. Liu, B.L. Xiao, W.G. Wang, Z.Y. Ma, Singly dispersed carbon nanotube/aluminum composites fabricated by powder metallurgy combined with friction stir processing, Carbon 50 (5) (2012) 1843–1852.
[26] Z.Y. Liu, B.L. Xiao, W.G. Wang, Z.Y. Ma, Analysis of carbon nanotube shortening and composite strengthening in carbon nanotube/aluminum composites fabricated by multi-pass friction stir processing, Carbon 69 (2) (2014) 264–274.
[27] K. Zhao, Z.Y. Liu, B.L. Xiao, D.R. Ni, Z.Y. Ma, Origin of insignificant strengthening effect of CNTs in T6-treated CNT/6061Al composites, Acta Metall. Sin. 31 (2018) 134–142.
[28] F. Khodabakhshi, S.M. Arab, P. Svec, A.P. Gerlich, Fabrication of a new Al-Mg/graphene nanocomposite by multi-pass friction stir processing: dispersion, microstructure, stability, and strengthening, Mater. Char. 132 (2017) 92–107.
[29] S.C. Tjong, Recent progress in the development and properties of novel metal matrix nanocomposites reinforced with carbon nanotubes and graphene nanosheets, Mater. Sci. Eng. R 74 (2013) 181–350.
[30] A.C. Ferrari, J. Robertson, Interpretation of Raman spectra of disordered and amorphous carbon, Phys. Rev. B 61 (2000) 14095–14107.
[31] T.M.G. Mohiuddin, A. Lombardo, R.R. Nair, A. Bonetti, G. Savini, R. Jalil, et al., Uniaxial strain in graphene by Raman spectroscopy: G peak splitting, gruneisen parameters, and sample orientation, Phys. Rev. B 79 (20) (2008) 196–198.
[32] R.S. Mishra, Z.Y. Ma, Friction stir processing: a novel technique for fabrication of surface composite, Mater. Sci. Eng., A 341 (2003) 307–310.
[33] W.W. Zhou, T. Yamaguchi, K. Kikuchi, N. Nomura, A. Kawasaki, Effectively enhanced load transfer by interfacial reactions in multi-walled carbon nanotube reinforced Al matrix composites, Acta Mater. 125 (2017) 369–376.
[34] M. Rashad, F. Pan, A. Tang, M. Asif, Effect of graphene nanoplatelets addition on mechanical properties of pure aluminum using a semi-powder method, Prog Nat Sci Mat Int 24 (2014) 101–108.
[35] J.L. Tsai, T.C. Lu, Investigating the load transfer efficiency in carbon nanotubes reinforced nanocomposites, Compos. Struct. 90 (2) (2009) 172–179.
[36] R. Zhong, H. Cong, P. Hou, Fabrication of nano-Al based composites reinforced by single-walled carbon nanotubes, Carbon 41 (2003) 848–851.
[37] S.J. Yan, S.L. Dai, X.Y. Zhang, C. Yang, Q.H. Hong, J.Z. Chen, et al., Investigating aluminum alloy reinforced by graphene nanoflakes, Mater. Sci. Eng., A 612 (33) (2014) 440–444.
[38] Z.Y. Liu, B.L. Xiao, W.G. Wang, Z.Y. Ma, Developing high-performance aluminum matrix composites with directionally aligned carbon nanotubes by combining friction stir processing and subsequent rolling, Carbon 62 (5) (2013) 35–42.
[39] Q. Liu, L. Ke, F. Liu, C. Huang, L. Xing, Microstructure and mechanical property of multi-walled carbon nanotubes reinforced aluminum matrix composites fabricated by friction stir processing, Mater. Des. 45 (45) (2013) 343–348.